

The Macrophage Mediates the Renoprotective Effects of Endotoxin Preconditioning

Takashi Hato,* Seth Winfree,* Rabih Kalakeche,* Shataakshi Dube,* Rakesh Kumar,* Momoko Yoshimoto,^{†‡} Zoya Plotkin,* and Pierre C. Dagher*

Departments of *Medicine and [†]Pediatrics and [‡]The Wells Center for Pediatric Research, Indiana University, Indianapolis, Indiana

ABSTRACT

Preconditioning is a preventative approach, whereby minimized insults generate protection against subsequent larger exposures to the same or even different insults. In immune cells, endotoxin preconditioning downregulates the inflammatory response and yet, preserves the ability to contain infections. However, the protective mechanisms of preconditioning at the tissue level in organs such as the kidney remain poorly understood. Here, we show that endotoxin preconditioning confers renal epithelial protection in various models of sepsis *in vivo*. We also tested the hypothesis that this protection results from direct interactions between the preconditioning dose of endotoxin and the renal tubules. This hypothesis is on the basis of our previous findings that endotoxin toxicity to nonpreconditioned renal tubules was direct and independent of immune cells. Notably, we found that tubular protection after preconditioning has an absolute requirement for CD14-expressing myeloid cells and particularly, macrophages. Additionally, an intact macrophage CD14-TRIF signaling pathway was essential for tubular protection. The preconditioned state was characterized by increased macrophage number and trafficking within the kidney as well as clustering of macrophages around S1 proximal tubules. These macrophages exhibited increased M2 polarization and upregulation of redox and iron-handling molecules. In renal tubules, preconditioning prevented peroxisomal damage and abolished oxidative stress and injury to S2 and S3 tubules. In summary, these data suggest that macrophages are essential mediators of endotoxin preconditioning and required for renal tissue protection. Preconditioning is, therefore, an attractive model to investigate novel protective pathways for the prevention and treatment of sepsis.

J Am Soc Nephrol 26: 1347–1362, 2015. doi: 10.1681/ASN.2014060561

Gram-negative sepsis is a formidable and challenging clinical condition that carries very high morbidity and mortality. Indeed, it is estimated that mortality from sepsis can exceed 70%, especially when complicated by organ failure.¹ AKI is frequently seen in patients with sepsis and dramatically increases morbidity and mortality. To date, treatment of sepsis and sepsis-induced AKI remains supportive and relies primarily on antibiotic therapy, fluid and electrolyte management, and hemodynamic support.²

One hallmark of sepsis is widespread tissue oxidative stress. Uncontrolled reactive oxygen species rapidly react with all biologic macromolecules and result in deleterious tissue damage,

including organ failure. We and others have shown that the endotoxin (LPS) receptor Toll-like receptor 4 (TLR4) and coreceptor CD14 are expressed in renal tubules and upregulated in sepsis and ischemia.^{3–8} We also showed that systemic endotoxin is freely filtered and interacts with S1

Received June 10, 2014. Accepted July 27, 2014.

Published online ahead of print. Publication date available at www.jasn.org.

Correspondence: Dr. Pierre C. Dagher, Division of Nephrology, 950 West Walnut Street, R2-202A, Indianapolis, IN 46202. Email: pdaghe2@iupui.edu

Copyright © 2015 by the American Society of Nephrology

proximal tubules through a TLR4- and CD14-dependent mechanism. This interaction results in severe oxidative stress and peroxisomal damage in downstream tubular segments S2 and S3. Importantly, we showed that the interactions between endotoxin and S1 causing oxidative stress occur even in the absence of endotoxin-responsive hematopoietic cells.⁹

Preconditioning is a preventative approach in which pretreatment with controlled and minimized insults generates protection against subsequent larger exposures to the same or even different insults.^{10,11} Endotoxin preconditioning has been studied primarily at the level of immune cells, where it causes phenotypic changes favoring reduced inflammatory responses on endotoxin re-exposure. Furthermore, preconditioned immune cells also upregulate a broad class of antimicrobial and cytoprotective effectors. Collectively, these data indicate that endotoxin preconditioning is a complex and highly regulated gene reprogramming process.¹² Therefore, preconditioning is a unique and attractive model to investigate potential pathways that ensure effective microbial containment along with reduced collateral tissue damage from poorly targeted inflammation. Note that protective preconditioning as investigated in this work is fundamentally different from the deleterious Shwartzman reaction. The latter is typically elicited by consecutive intradermal or intravenous (iv) endotoxin injections and results in disseminated intravascular coagulation, exaggerated cytokine surge, and tissue necrosis.¹³ Protective endotoxin preconditioning and the Shwartzman reaction differ primarily in the route of endotoxin exposure.

The term endotoxin tolerance is avoided in this work, because it has resulted in substantial confusion in this field. The term tolerance is not universally defined and frequently used to describe the state of dysregulated global immunosuppression observed in the late phases of severe sepsis.¹⁴ The phenomenon of preconditioning investigated herein results in protection without concomitant immunosuppression. In fact, a few studies have shown increased survival in various models of sepsis after preconditioning.^{15–17}

In this study, we investigate the effectiveness and mechanisms of endotoxin preconditioning at the level of the intact kidney *in vivo*. In particular, the functional importance of renal epithelial cells in this process is poorly understood.^{18–21} Our recent findings that endotoxin-induced oxidative stress can result from direct endotoxin–tubule interaction raised the possibility that preconditioning is also a local renal event that is independent from hematopoietic cells. Surprisingly and in contrast to the direct endotoxin-induced tubular toxicity observed in the nonpreconditioned kidney, we find that preconditioning-induced renal protection has an absolute requirement for fully functional macrophages. Our understanding of the molecular and cellular mechanisms of endotoxin preconditioning *in vivo* could lead to novel approaches for the prevention and treatment of sepsis and sepsis-induced AKI.

RESULTS

Endotoxin-Induced Tubular Injury Is Independent of Immune Cells and Immune Cell-Derived Inflammatory Cytokines

As a prelude to our investigation of preconditioning, we show in Figure 1 that endotoxin toxicity to the nonpreconditioned kidney has no requirement for endotoxin-responsive hematopoietic cells. Indeed, as shown in Figure 1, C–E, endotoxin caused severe tubular oxidative stress and an increase in the tubular injury markers kidney injury molecule-1 (KIM-1) and neutrophil gelatinase-associated lipocalin (NGAL) in bone marrow chimeras lacking endotoxin-responsive hematopoietic cells (TLR4^{-/-} into wild-type [WT] animals; knockout [KO]/WT). In contrast, the reverse WT/KO chimera, which has competent immune cells but lacks tubular TLR4, had no tubular injury. Note that, in these chimeras, >96% of all immune cells in the bone marrow, circulation, and kidneys were replaced by the donor cells (Figure 1B), excluding the possibility that tubular injury is mediated by residual competent immune cells in the KO/WT chimera. The injury-resistant WT/KO chimera had the highest levels of serum and renal cytokines and chemokines (Figure 1, F and G). This indicates that these cytokines and chemokines are primarily immune cell-derived and do not correlate with the degree of tubular injury. This is consistent with our previous findings⁹ that endotoxin-induced tubular injury in the nonpreconditioned kidney is a local event.

Renal Tubules Become Resistant to Endotoxin-Induced Oxidative Stress after Preconditioning

We have previously shown that systemically administered endotoxin is filtered and internalized by S1 proximal tubules in a TLR4-dependent mechanism.⁹ This results in oxidative stress in the downstream S2 and S3 segments as early as 4 hours after endotoxin. Oxidative stress was seen throughout the tubular cell cytoplasm and particularly prominent at the brush border. S1 tubules showed no oxidative stress at any time point. Our measurements of oxidative stress with 2',7'-dichlorodihydrofluorescein diacetate (H₂DCFDA) were rigorously validated by confirming probe loading into all tubules as well as duplication of the results with different probes, such as dihydroethidium (Supplemental Figure 1) (supplemental figure 2 in ref. 9). Here, we examined whether preconditioning protects the tubules *in vivo* and curtails endotoxin-induced oxidative stress. We found that pre-exposure to low-dose endotoxin completely abolishes tubular oxidative stress after high-dose endotoxin (Figure 2, A–D). In fact, the degree of protection was comparable with that seen in the naturally endotoxin-resistant TLR4^{-/-} mice (Figure 2E).

Remarkably, this tubular protection occurs despite the increased TLR4-dependent uptake of endotoxin, which is induced by preconditioning (Figure 2F). This indicates that S2 and S3 tubular protection is not secondary to reduced S1 tubular endotoxin uptake. In addition, endotoxins from rough and smooth bacterial strains were comparable in inducing successful preconditioning (Figure 2G). In summary,

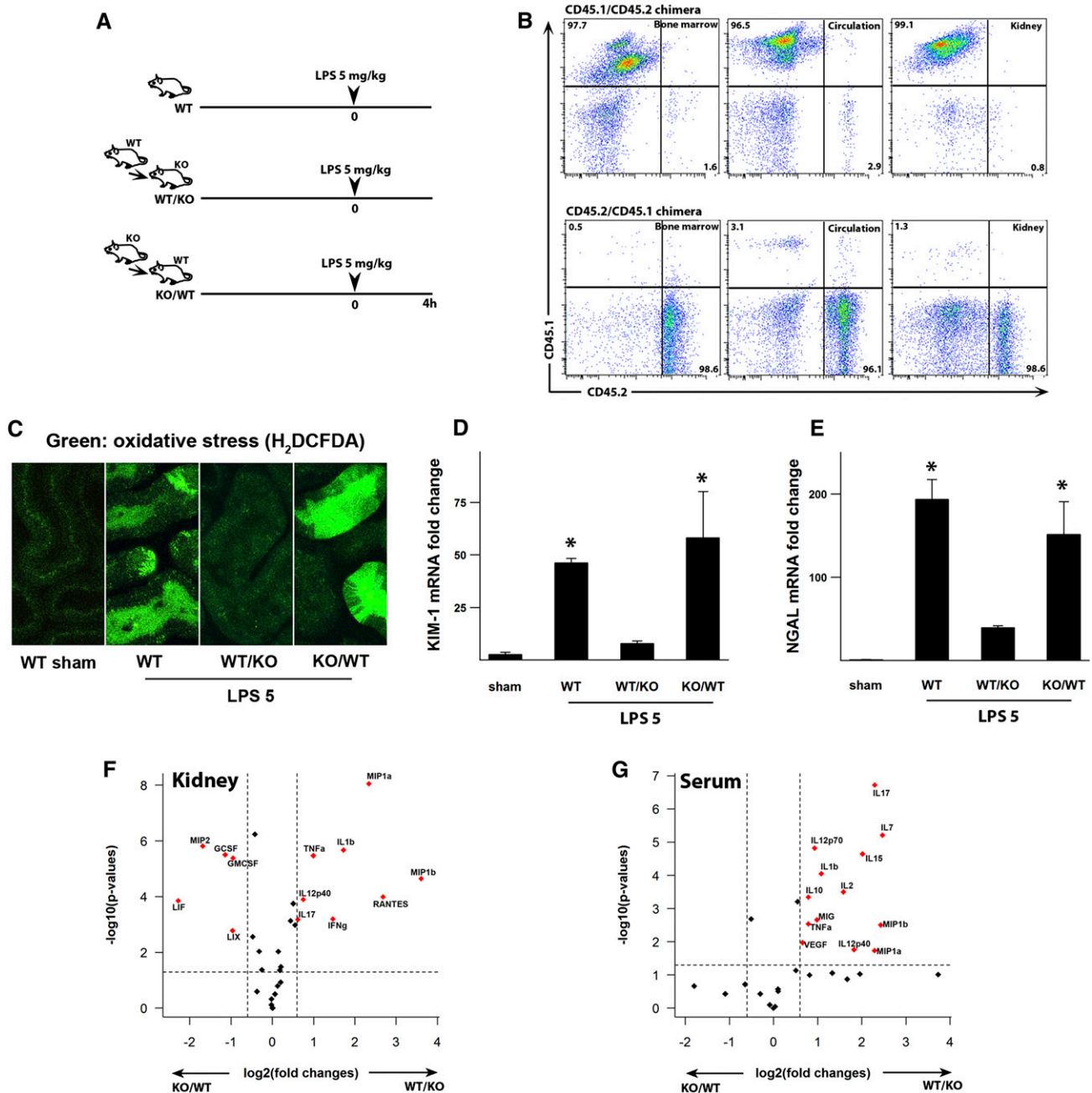


Figure 1. LPS-induced tubular injury is mediated by tubular TLR4. (A) Experimental strategy is shown. Animals were injected with 5 mg/kg LPS ip. (B) BoyJ (CD45.1) and C57BL/6 (CD45.2) bone marrow chimeras were generated to assess the degree of chimerism 8 weeks after irradiation. It exceeded 96% of total $CD45^+$ cells in all tissues (percentages of upper left, upper right, and lower right panels). (C) TLR4 chimeric mice were generated through bone marrow transfer from WT into TLR4^{-/-} mice (WT/KO) or from TLR4^{-/-} to WT mice (KO/WT). Oxidative stress was measured with H_2DCFDA (green) using two-photon intravital microscopy. Measurements were performed 4 hours after 5 mg/kg LPS (LPS 5) or vehicle control (sham). Oxidative stress was observed in proximal tubules of WT animals and KO/WT chimeric mice but not the reverse chimeras (WT/KO). (D and E) The degree of tubular injury was determined with KIM-1 and NGAL mRNA levels of kidney tissues after 5 mg/kg LPS ip and normalized to GAPDH. * $P < 0.05$ versus sham or WT/KO. (F and G) Volcano plots of kidney and serum cytokine/chemokine multiplex panels. Kidney tissue and serum were obtained 4 hours after 5 mg/kg LPS ip. The dashed lines denote $P = 0.05$ (y axis) and 1.6-fold change (x axis). Positive value fold change indicates that WT/KO > KO/WT (e.g., a position $[x, y] = [2, 2]$ indicates a 4-fold increase in WT/KO compared with KO/WT with a P value = 0.01). $n = 3$ per group. GAPDH, glyceraldehyde-3-phosphate dehydrogenase

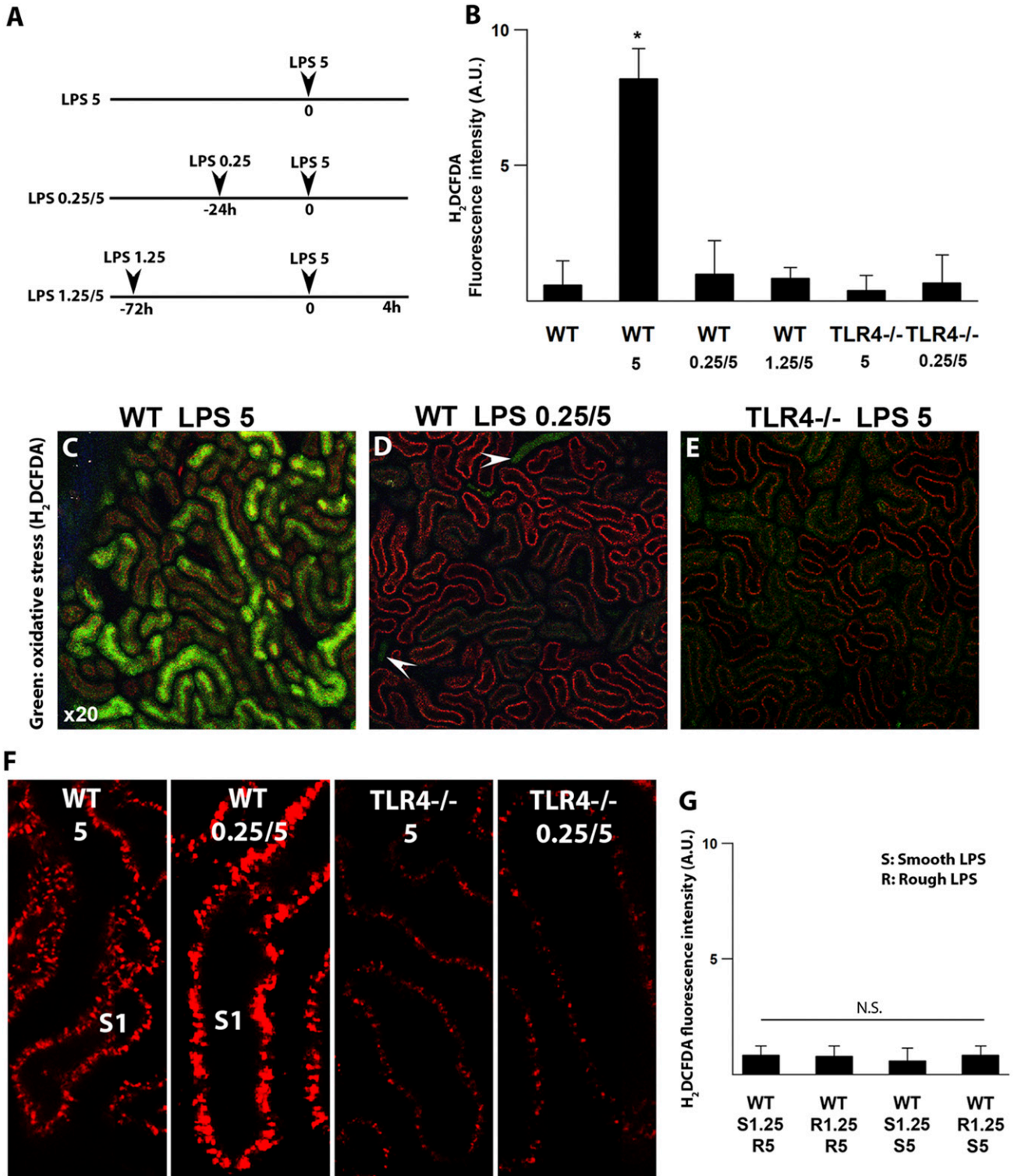


Figure 2. Preconditioning abrogates endotoxin-induced tubular oxidative stress. (A) Preconditioning strategy consisted of 0.25 or 1.25 mg/kg unlabeled LPS ip followed by fluorescently labeled 5 mg/kg LPS (red) ip as denoted. Nonpreconditioned mice were subjected to a single dose of 5 mg/kg LPS ip. (B–E) Oxidative stress was measured with carboxy-H₂DCFDA (green) using two-photon intravital imaging. Measurements were performed 4 hours after 5 mg/kg LPS. After 5 mg/kg LPS, prominent oxidative stress was observed in proximal tubules of nonpreconditioned WT animals (LPS 5), whereas oxidative stress was absent in preconditioned WT mice (LPS 0.25/5 and LPS 1.25/5). TLR4^{-/-} mice showed no oxidative stress under all conditions. Arrowheads point to luminal H₂DCFDA concentrated in collecting ducts, confirming agent delivery. Quantitation of oxidative stress under the indicated conditions is shown in B. **P*<0.05

preconditioning a host with low-dose endotoxin can abrogate oxidative stress in renal epithelial cells *in vivo*.

Endotoxin Preconditioning Prevents Peroxisomal Damage in Renal Tubules

We have previously shown that endotoxin-induced tubular oxidative stress correlated best with early and severe peroxisomal damage. This preceded any measurable injury to mitochondria.⁹ Indeed, peroxisomes are abundant in S2 and S3 segments (but not S1) and involved in several oxidative metabolic pathways.²² When damaged, peroxisomes can be a major source of pathologic reactive species.^{23,24} Here, we show that endotoxin preconditioning prevents peroxisomal damage as assessed by the peroxisomal antioxidant enzymes catalase and peroxiredoxin5 (Prdx5) (Figure 3, A–F). We confirmed the upregulation of Prdx5 by unbiased two-dimensional gel proteomics (Figure 3G, Supplemental Figure 2, Supplemental Table 1). We also examined NADPH oxidase 4 (Nox4), an enzyme involved in redox pathways and heavily expressed in the tubular brush border, as a potential source of endotoxin-induced oxidative stress. Our data show that Nox4 expression was unchanged under all conditions (Figure 3H).

Preconditioning Prevents Tubular Injury in Multiple Models of Sepsis

Next, we examined whether the early abrogation of peroxisomal damage and oxidative stress by preconditioning translated into actual protection as measured by traditional renal and tubular injury markers. In the endotoxemia model, we show that preconditioning does, indeed, result in functional renal protection with reduced BUN as well as a significant reduction in the tubular injury markers KIM-1 and NGAL (Figure 4, A–C). Importantly, we show that preconditioning is also protective in models of actual bacterial infections, such as polymicrobial cecal ligation and puncture and live *Escherichia coli* infusion (Figure 4, D–F). These data support a model in which abrogation of oxidative stress by preconditioning confers renal protection in various animal models of sepsis.

The Renoprotective Effects of Preconditioning Require Hematopoietic Cells Expressing TLR4

As shown in Figure 1, endotoxin toxicity to the nonpreconditioned kidney has no requirement for hematopoietic cells. Here, we investigated whether the protective effects of preconditioning are also hematopoietic cell-independent. To this end, we examined TLR4KO/WT chimeras that lack endotoxin-responsive hematopoietic cells including those present in the kidney. Surprisingly, these chimeras failed two separate preconditioning regimens and exhibited severe tubular oxidative

stress after 5-mg/kg LPS challenge (Figure 5, Supplemental Figure 3, KIM-1 expression levels). Therefore, unlike acute toxicity to the nonpreconditioned kidney, TLR4-expressing hematopoietic cells are essential for successful preconditioning. Note that the reverse WT/TLR4KO chimera is not susceptible to endotoxin injury, and therefore, preconditioning could not be evaluated (Figure 1, C–E).

The Renoprotective Effects of Preconditioning Require CD14-Expressing Macrophages

Although TLR4 is the primary endotoxin receptor, its coreceptor CD14 is required for optimal sensing and uptake of endotoxin.²⁵ We, therefore, examined preconditioning in chimeric mice lacking hematopoietic CD14. Like TLR4 chimeras, chimeras lacking hematopoietic CD14 also failed to mount protective preconditioning (Figure 6, A and B).

We next investigated whether this failure is related to dysfunctional TIR domain-containing adapter-inducing interferon- β (TRIF) signaling. Downstream of TLR4, the myeloid differentiation primary response gene 88- (MyD88-) and Toll-IL-1 receptor domain containing adaptor protein inducing the IFN beta- (TRIF) signaling pathways can be differentially stimulated by various bacterial endotoxins. CD14 is required for signaling through TRIF,²⁶ a pathway recently shown to be involved in macrophage endotoxin preconditioning.^{27,28} We, therefore, investigated whether polyinosinic:polycytidylic acid [poly (I:C)], an agonist of TLR3 that signals exclusively through TRIF, could restore the protective effects of preconditioning in the CD14KO/WT chimeras. As shown in Figure 6C, poly (I:C) partially restored the protective effects of preconditioning in the CD14KO/WT chimeras. This suggests that the TRIF pathway participates in the mechanism of preconditioning but that the actual presence of CD14 is essential for complete protection. Note that poly (I:C) was administered simultaneously with 0.25 mg/kg endotoxin so that both MyD88- and TRIF-signaling pathways can be activated in the absence of CD14. Poly (I:C) given alone without endotoxin pre-exposure in CD14KO/WT chimeras failed to induce preconditioning and protection (not shown). This indicates that concurrent activation of MyD88 along with TRIF is required for successful preconditioning.

CD14 is highly expressed in monocytes and macrophages. We, therefore, investigated whether an intact macrophage CD14-TRIF pathway is essential for preconditioning. To this end, we fluorescently labeled poly (I:C) and localized it in kidneys of preconditioned CX₃CR1-EGFP mice. This mouse expresses EGFP in myeloid cells, such as dendritic cells and macrophages, but not neutrophils.²⁹ By two-photon intravital microscopy, three EGFP-expressing cell types can be seen in the kidneys of

versus other experimental groups. *n*=4 per group. (F) Preconditioning enhanced LPS internalization (red) by S1 proximal tubules in WT animals. LPS uptake observed in TLR4^{-/-} mice is secondary to fluid-phase endocytosis. (G) Rough and smooth LPSs were equally successful in preconditioning. *E. coli* 0111:B4 (smooth LPS; highly glycosylated; denoted as S) and *S. minnesota* R595 (rough LPS; poorly glycosylated; denoted as R) were used in various combinations.

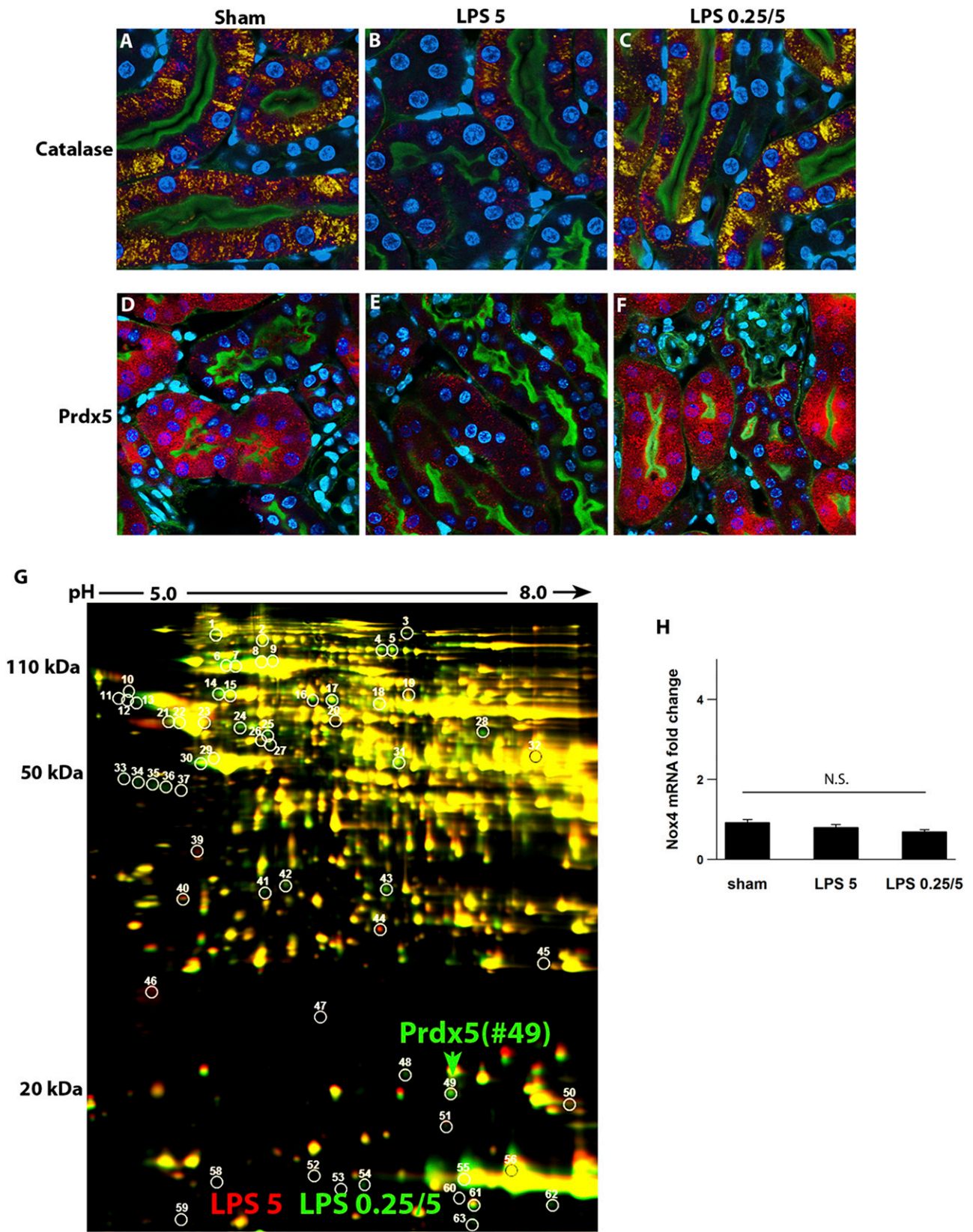


Figure 3. Preconditioning prevents endotoxin-induced peroxisomal damage. (A–F) Fluorescence microscopy of fixed kidney sections from animals treated with indicated conditions and immunostained for catalase (yellow) or Prdx5 (red). Nuclei were stained blue with DAPI. Green is FITC-phalloidin staining of the apical brush border. Four hours after LPS (5 mg/kg), the expressions of peroxisomal

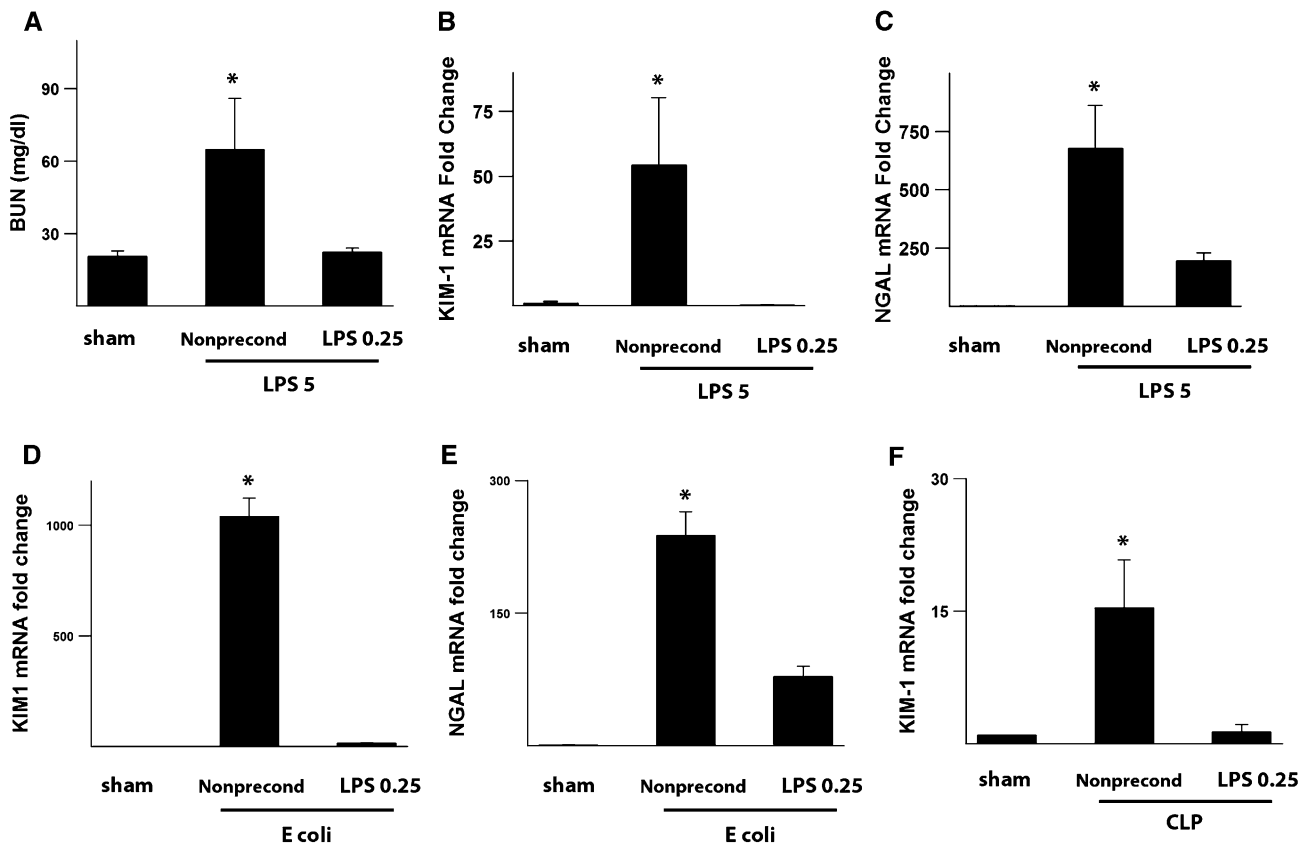


Figure 4. Preconditioning attenuates tubular injury in various models of sepsis. (A–C) BUN as well as KIM-1 and NGAL mRNA levels of kidney tissues measured 24 hours after 5 mg/kg LPS. KIM-1 and NGAL expression levels were normalized to GAPDH. (D and E) Animals were injected with 1 million live *E. coli* iv alone (nonpreconditioned) or 0.25 mg/kg LPS ip followed 24 hours later by *E. coli* iv (preconditioned). (F) Animals were subjected to cecal ligation and puncture (CLP) alone (nonpreconditioned) or 0.25 mg/kg LPS ip followed 24 hours later by CLP (preconditioned). Kidney tissue KIM-1 levels were measured 24 hours after CLP in both groups. $n=4$ per group. $*P<0.05$ versus other experimental groups. GAPDH, glyceraldehyde-3-phosphate dehydrogenase.

this mouse: (1) sessile dendritic cells easily recognized by their shape and high levels of EGFP, (2) mobile macrophages expressing high EGFP, and (3) mobile macrophages expressing intermediate EGFP. As shown in Figure 6E, fluorescently labeled poly (I:C) localized exclusively to the macrophage subset with intermediate EGFP expression. This supports an essential role for macrophage subsets in mediating endotoxin preconditioning.

Finally, we confirmed the essential role of macrophages using a clodronate depletion model. As shown in Figure 6, F and G, clodronate was effective in depleting macrophages. Mice treated with clodronate failed to mount renal protection after preconditioning (Figure 6H, Supplemental Figure 4).

In contrast to chimeric mice, the investigation of endotoxin preconditioning in total CD14- or TRIF-KO animals is

complicated by their natural partial resistance to endotoxin toxicity. Nevertheless, endotoxin preconditioning not only failed to induce tissue protection but even caused increased toxicity, especially in the CD14^{-/-} mouse (Supplemental Figures 5–7). In summary, successful renal tubular preconditioning requires CD14-expressing macrophages.

Kidneys of Preconditioned Mice Show Increased Macrophage Number and M2 Polarization

In preconditioned kidneys, we observed a significant increase in the number of F4/80-positive macrophages. This increase could be detected in the preconditioned group as early as 4 hours after 5 mg/kg endotoxin (Figure 7, A–D). By flow cytometry, these macrophages showed a significant increase in the

antioxidant enzymes catalase and Prdx5 were decreased in nonpreconditioned mice but well preserved in preconditioned mice. (G) The preserved expression of Prdx5 in the preconditioned kidney was also identified by unbiased two-dimensional difference gel electrophoresis of kidney extracts (spot 49) and correlated well with tissue Prdx5 staining (red, nonpreconditioned; green, preconditioned). Supplemental Figure 2 and Supplemental Table 1 show the Prdx5 identification summary. (H) Whole-kidney Nox4 levels were comparable among all conditions as determined by quantitative PCR (normalized to GAPDH). DAPI, 4',6-diamidino-2-phenylindole; GAPDH, glyceraldehyde-3-phosphate dehydrogenase.

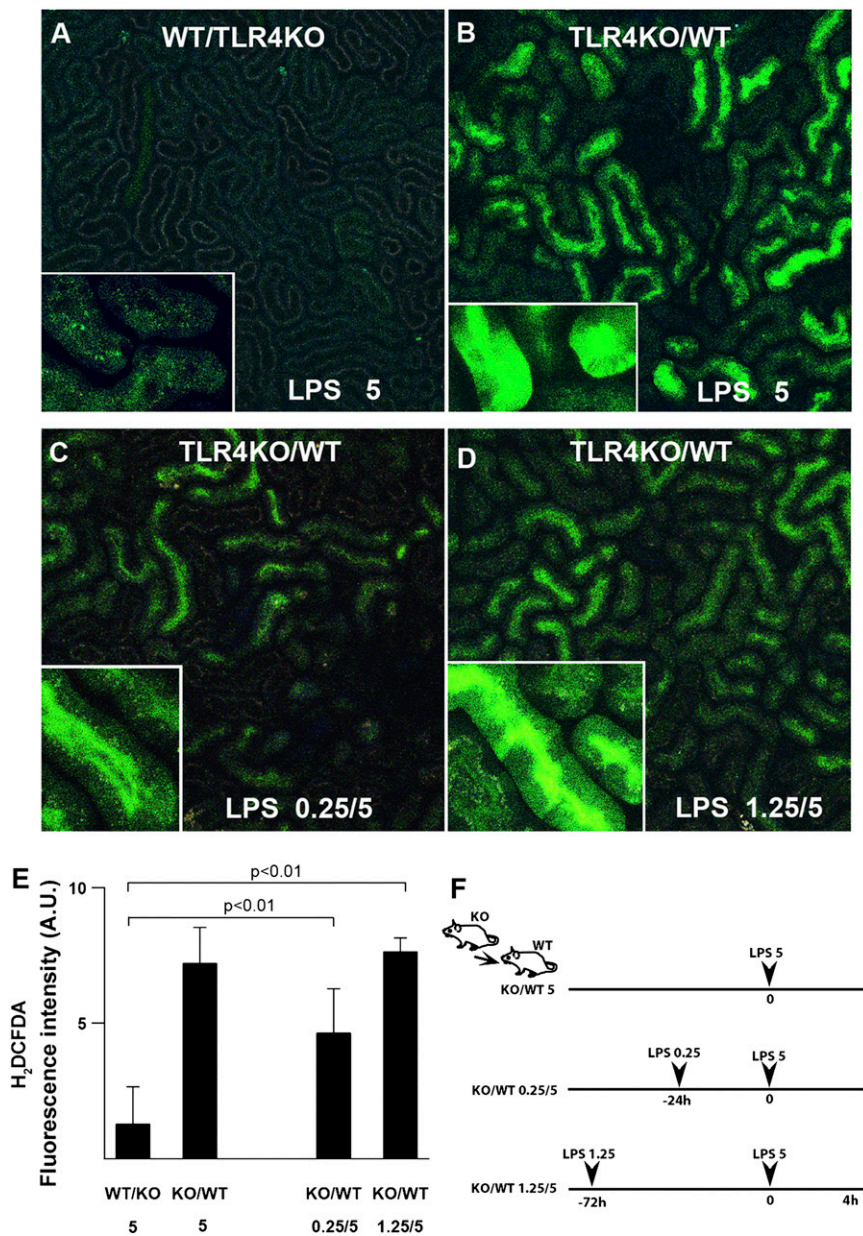


Figure 5. Hematopoietic TLR4 is essential for protective tubular preconditioning. Chimeric mice were generated through bone marrow transfer from WT to TLR4^{-/-} mice (WT/TLR4KO) or from TLR4^{-/-} to WT mice (TLR4KO/WT). The degree of tubular oxidative stress (green; oxidized H₂DCFDA) was determined with intravital microscopy 4 hours after 5 mg/kg LPS ip. (A and B) In the absence of LPS preconditioning, a single dose of 5 mg/kg LPS caused oxidative stress in TLR4KO/WT but not WT/TLR4KO chimeras. (C and D) After LPS preconditioning, TLR4KO/WT chimeric mice failed to mount tubular protection. (E) Quantitation of oxidative stress under the indicated conditions. (F) Experimental strategy is shown.

CD206-positive fraction. CD206, also known as the mannose receptor, is a phagocytic receptor for bacteria and a marker of the alternatively activated M2 macrophages (Figure 7, E–G, Supplemental Figure 8). Note that this macrophage accumulation did not result in increased tissue inflammation (Figure 7H). In addition, changes in neutrophil Gr-1 and terminal deoxynucleotidyl

transferase-mediated digoxigenin-deoxyuridine nick-end labeling staining were minimal between nonpreconditioned and preconditioned groups (Supplemental Figure 9). We also examined other leukocyte profiles in the kidney. Endotoxin pre-exposure tended to reduce renal CD4, CD8, and B lymphocyte numbers while increasing natural killer cells (Supplemental Figure 10).

Macrophages in the Kidneys of Preconditioned Mice Have Increased Expression of Heme Oxygenase 1 and Sirtuin 1

Heme oxygenase 1 (HO1) and sirtuin 1 (SIRT1) are cytoprotective molecules that can profoundly modulate myeloid cell biology in response to endotoxin.^{30–38} In particular, HO1 is essential for the regulation of redox pathways and catabolism of heme.^{31,39} Here, we show that endotoxin preconditioning upregulated HO1 and SIRT1 in F4/80-positive macrophages (Figure 8). We also noted an increase in HO1 and SIRT1 in renal tubules of preconditioned mice. However, TLR4KO/WT chimeras also showed increased expression of HO1 and SIRT1 in tubules but not interstitial macrophages (Supplemental Figure 11). These TLR4KO/WT chimeras failed to develop protective preconditioning, indicating that tubular HO1 and SIRT1 may not be sufficient for tubular protection in the absence of macrophage HO1 and SIRT1.

The overall importance of HO1 and other iron-handling molecules in attaining tissue protection is further shown by a marked increase in the expression of hemopexin, transferrin, and haptoglobin in sera from preconditioned mice (Figure 9, Supplemental Figure 2, Supplemental Table 2).

Preconditioning Increases the Activity and Trafficking of Macrophages in the Kidney

We took advantage of poly (I:C) labeling of the EGFP-intermediate macrophage subset to investigate trafficking and activity [without poly (I:C) labeling, the low EGFP fluorescence of these cells precludes accurate tracking because of tubular autofluorescence]. We show in Figure 10, A and B that the kidneys of preconditioned mice exhibited a large number of poly (I:C)-labeled macrophages with increased activity. This activity included trafficking between tubules and frequent contact with dendritic cells, other macrophages, and tubules. In contrast, kidneys from nonpreconditioned mice

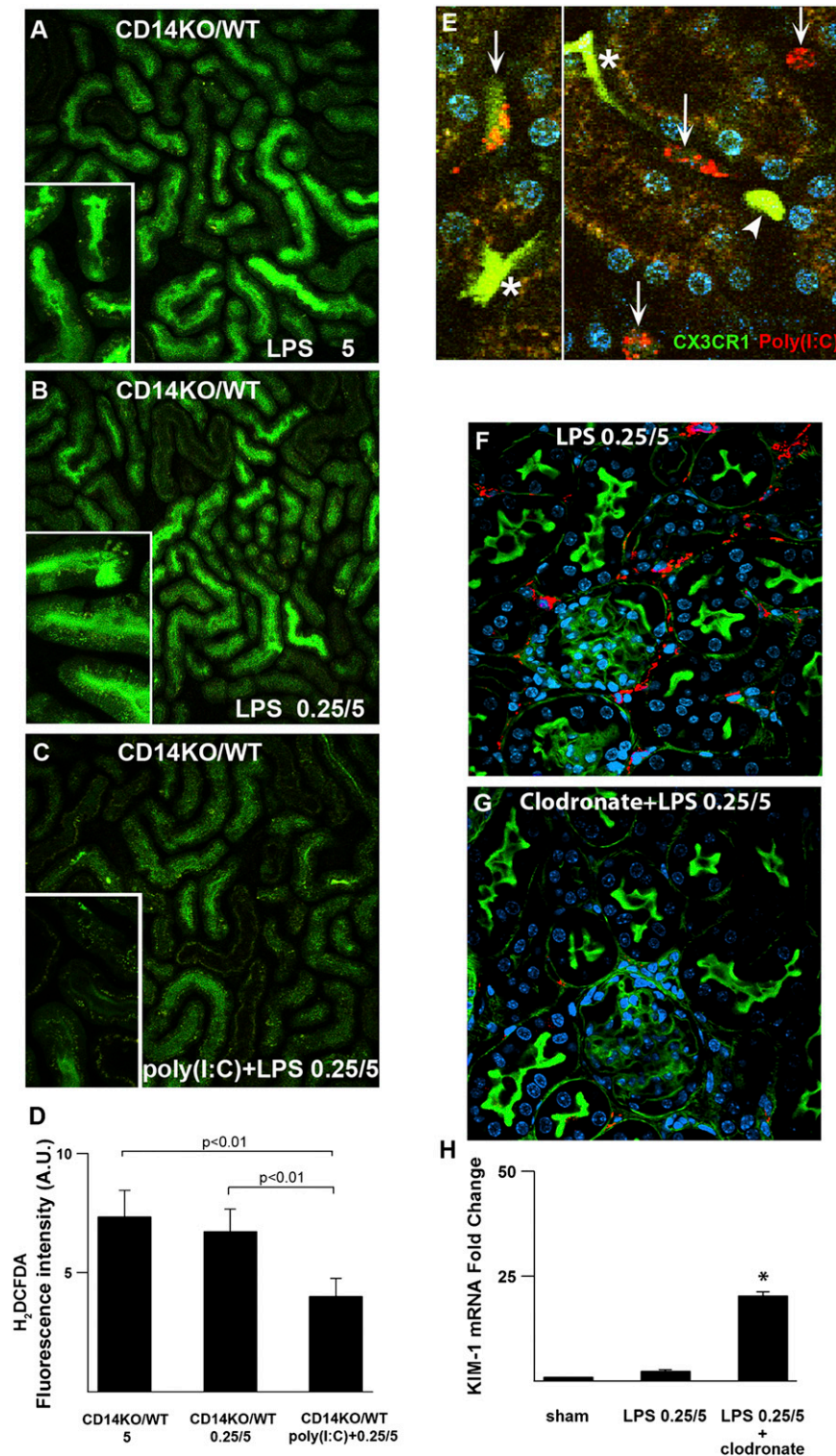


Figure 6. Macrophage CD14 is indispensable for protective tubular preconditioning. (A and B) Chimeric mice were generated through bone marrow transfer from CD14^{-/-} into WT mice (CD14KO/WT). Oxidative stress (green; oxidized H₂DCFDA) was measured 4 hours after 5 mg/kg LPS in nonpreconditioned and preconditioned animals. (B) Note the failure of preconditioned CD14KO/WT mice to mount tubular protection. (C and D) Poly (I:C) restored tubular protection to CD14KO/WT chimeras. (E) To localize poly (I:C), the CX₃CR1-EGFP mouse was injected with rhodamine-labeled poly

rarely showed poly (I:C)-labeled macrophages, and the overall activity and trafficking were minimal (Figure 10, C and D). Movies of macrophage activity and trafficking are shown in Supplemental Movies 1–6. The tracking of cells with heterogeneous cell body delineation and punctate signatures was made possible by developing a custom plugin for ImageJ. We made the source code publicly available (Supplemental Table 3).

We also show that, at later time points (72 hours after 5 mg/kg LPS), there is continued and widespread accumulation of macrophages in the preconditioned kidneys (Figure 10E). Compared with the 4-hour time point (Figure 7), macrophage numbers in the nonpreconditioned and preconditioned kidneys increased to 140 ± 15 and 190 ± 20 cells/field, respectively ($P < 0.05$, $n = 4$). The increased macrophage number was evident in both cortex and medulla. In preconditioned mice, these macrophages exhibited spatial clustering around S1 tubules, which occurred with high frequency throughout the cortex (70% of anatomically identifiable S1). No such clustering was observed in the kidneys of nonpreconditioned mice (Figure 10F, Supplemental Figure 12).

DISCUSSION

In this work, we investigated the powerful model of preconditioning with the purpose of identifying novel cellular and molecular pathways that can be protective in sepsis. Oxidative damage is recognized as one important pathophysiologic mechanisms of tissue injury in sepsis.^{40,41} Here, we identified

(I:C) (red) iv 20 minutes before intravital imaging. Preconditioned kidneys show sessile dendritic cells with high GFP fluorescence (asterisk) and mobile macrophages with either high GFP (arrowhead) or intermediate GFP fluorescence (arrows). Poly (I:C) localized to mobile macrophages express intermediate GFP. (F and G) Efficacy of clodronate-induced macrophage depletion is shown by immunostaining for F4/80 (red). (H) KIM-1 mRNA levels of kidney tissues measured 24 hours after 5 mg/kg LPS and normalized to GAPDH. * $P < 0.05$. GAPDH, glyceraldehyde-3-phosphate dehydrogenase; GFP, green fluorescent protein.

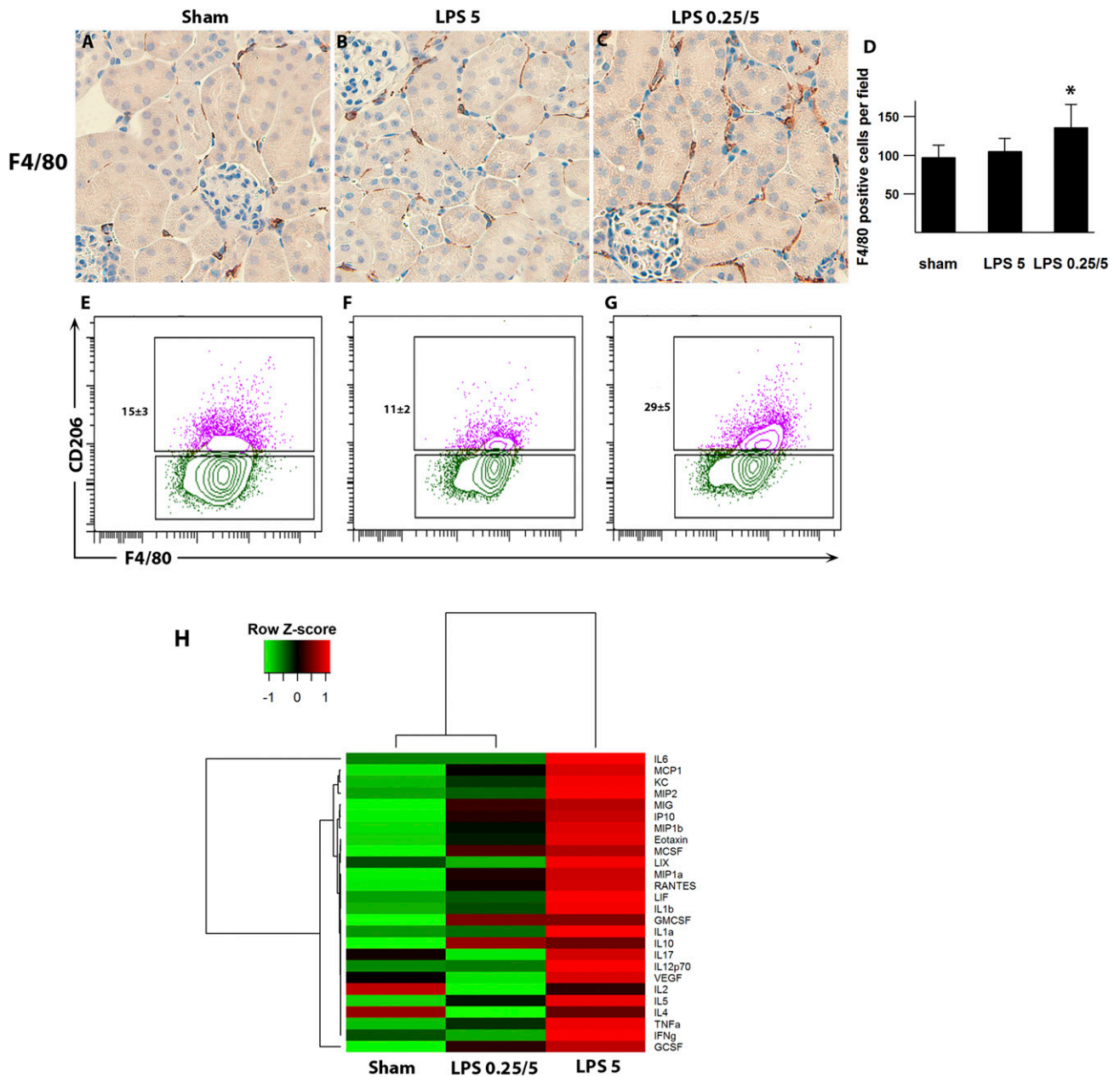


Figure 7. Preconditioning increases the number of macrophages in the kidney. (A–C) Representative images of F4/80 staining (brown; a marker of macrophages) are shown 4 hours after 5 mg/kg LPS. (D) The preconditioned group had significantly higher numbers of F4/80-positive cells compared with the nonpreconditioned group. * $P < 0.05$. (E–G) Flow cytometric analyses of kidney macrophages gated on CD45⁺CD11b⁺F4/80⁺ cells. CD206 (mannose receptor 1; a phagocytic receptor for microbes) is a marker of M2 macrophage phenotype. Representative dot plots show an increased percentage of M2 macrophages in preconditioned kidneys compared with nonpreconditioned kidneys or WT sham animals ($P < 0.01$ for preconditioned animals versus other experimental groups). Gating strategy is shown in Supplemental Figure 6. Kidneys were harvested 4 hours after 5 mg/kg LPS or vehicle treatment. $n = 3$ per group. (H) Heat map of kidney cytokine and chemokine levels. Analysis of kidney homogenate cytokines and chemokines was performed using multiplex magnetic bead panels. The values were log₂-transformed and scaled in the row direction. Analytes that did not reach $P < 0.01$ by ANOVA are not shown.

macrophages as important and essential mediators of protection against endotoxin-induced oxidative stress and renal tubular damage. Importantly, these macrophages exhibited upregulation of redox and iron-handling molecules. This is a novel finding and

indicates a potential role for these immune cells in kidney protection. In fact, it is now recognized that the late stages of sepsis are characterized by profound immunosuppression.^{42–44} This has prompted the search for new immunomodulatory

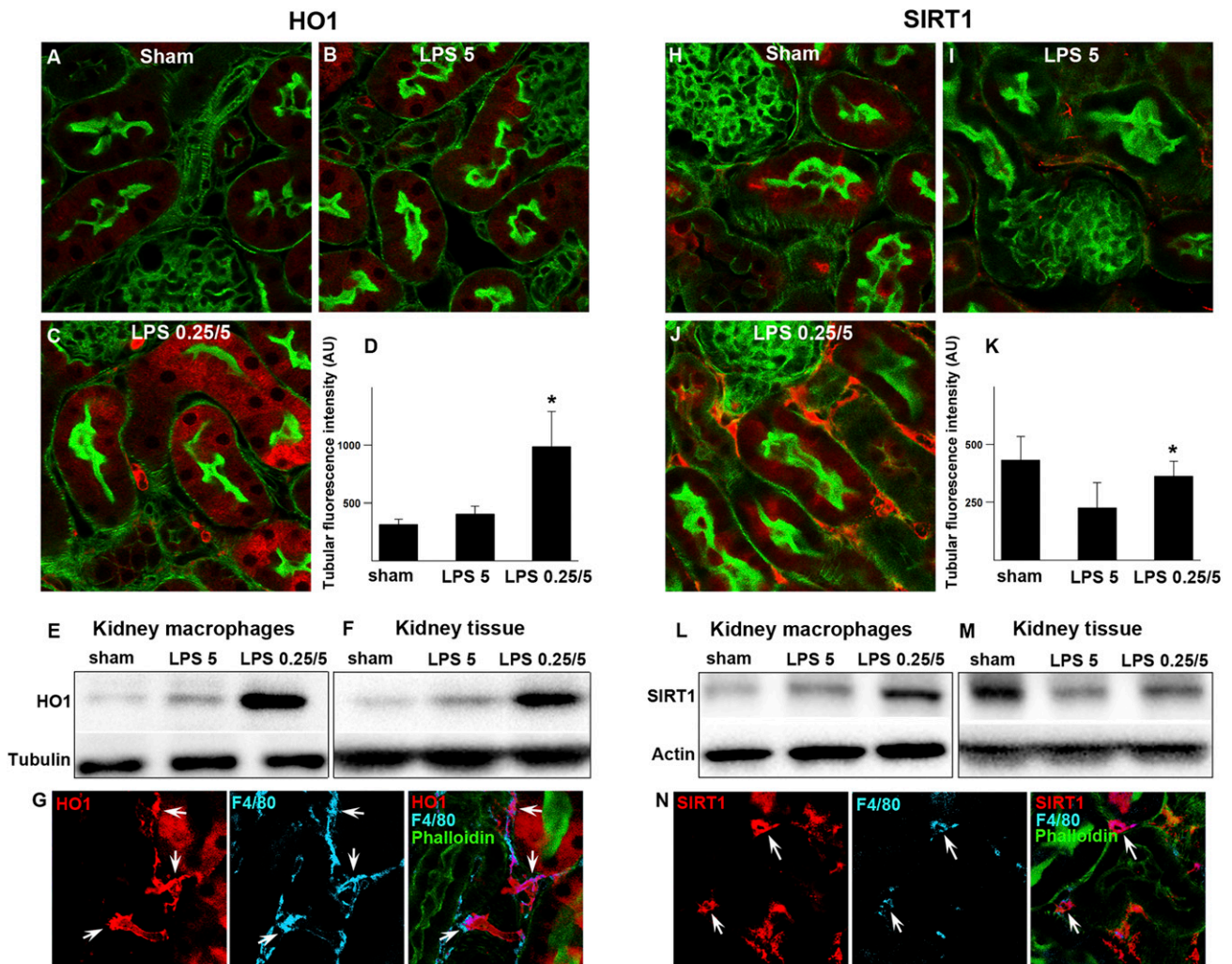


Figure 8. Preconditioning increases the renal expression of HO1 and SIRT1. (A–D) Fluorescence microscopy of fixed kidney sections from WT mice under indicated conditions and immunostained for HO1 (red) 4 hours after 5 mg/kg LPS. Green indicates FITC-phalloidin. (C) HO1 expression was markedly increased by preconditioning in myeloid cells and to a lesser degree, proximal tubular cells. (D) Quantitation of HO1 tubular fluorescence intensity. * $P < 0.05$ versus LPS 5. (E and F) Western blot analysis of HO1 in $CD11b^+F4/80^+$ macrophages isolated from kidneys under indicated conditions. The remaining negatively selected kidney tissue ($CD11b^-F4/80^-$) from the same animal was analyzed simultaneously. Western blot analysis of HO1 correlated well with tissue HO1 staining. Three animals were pooled for each condition. (G) Fixed kidneys were stained for HO1 (red) and costained with F4/80 (blue). Arrows point to interstitial cells coexpressing HO1 and F4/80. (H–K) Fluorescence microscopy of fixed kidney sections from WT mice under indicated conditions and immunostained for SIRT1 (red) 4 hours after 5 mg/kg LPS. (J) SIRT1 expression was markedly increased by preconditioning in myeloid or interstitial cells and to a lesser degree, tubules. (K) Quantitation of SIRT1 tubular fluorescence intensity. * $P < 0.05$ versus LPS 5. (L and M) Western blot analysis of SIRT1 expression in $CD11b^+F4/80^+$ macrophages cells isolated from kidneys under indicated conditions. The remaining negatively selected kidney tissue ($CD11b^-F4/80^-$) from the same WT animal was analyzed simultaneously. Western blot analysis of SIRT1 correlated well with tissue SIRT1 staining. Three animals were pooled for each condition. (N) Arrows point to interstitial cells coexpressing SIRT1 (red) and F4/80 (blue).

approaches to restore immune health.^{45–47} The protective macrophages that we describe here have the potential to serve such a purpose.

Recently, we showed that systemically administered endotoxin can directly interact with S1 proximal tubules and inflict severe peroxisomal damage and oxidative stress to downstream S2 and S3 tubular segments.⁹ These studies identified S1 as an

epithelial macrophage or epiphage with the ability to both sense and signal danger. Importantly, we showed that direct interactions between filtered endotoxin and S1 proximal tubules can cause downstream severe oxidative stress, even in chimeric mice lacking endotoxin-responsive hematopoietic cells. Because circulating hematopoietic cells are the major source of systemic cytokines (Figure 1), the observed damage

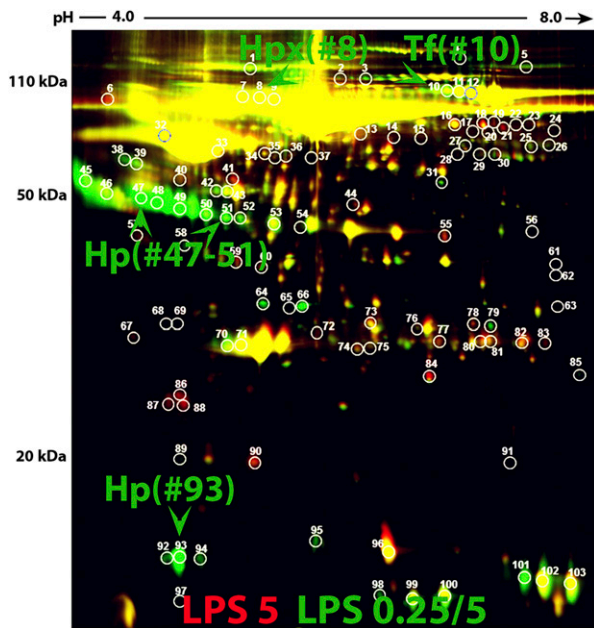


Figure 9. Preconditioning increases iron-related proteins in the serum. Serum haptoglobin (Hp), hemopexin (Hpx), and transferrin (Tf) were identified by two-dimensional difference gel electrophoresis followed by MS. Hp, Hpx, and Tf had at least 2-fold increases in the preconditioned animals (LPS 0.25/5; green) compared with nonpreconditioned animals (LPS5; red). Supplemental Figure 2 and Supplemental Table 2 show its protein identification summary.

in tubules was likely a local phenomenon resulting directly from endotoxin and S1 interactions.

In sharp contrast to tubular injury in the nonpreconditioned kidney, we show here that the protective effects of preconditioning are largely dependent on macrophages. These protective macrophages exhibit early increased activity and trafficking within the kidney and interact extensively with other myeloid cells and renal tubules. Interestingly, this activity culminated at later time points in macrophage clustering around the S1 tubules. The significance of this clustering remains to be determined. We speculate that it could represent specific crosstalk between macrophages and S1 tubules, the sites of endotoxin uptake. This crosstalk could downregulate S1 local proinflammatory signaling to downstream segments or conversely, upregulate protective molecular pathways. The molecular mechanisms of macrophage–S1 interactions remain to be determined.

We also show that protective macrophages exhibited increased expression of cytoprotective HO1 and SIRT1. Whether HO1 and SIRT1 are simply phenotypic macrophage markers or actually involved in the protective effects is unclear. It is possible that macrophages could serve as carriers of downstream molecules of HO1 and SIRT1 that can be delivered locally to specific microenvironments around the tubules and renal microvasculature. The potential importance of HO1 is underscored by the concurrent upregulation of molecules, such as haptoglobin and hemopexin, indicating an orchestrated response to control iron

and heme metabolism and their potential deleterious effects in sepsis. These molecules were identified by an unbiased proteomics approach. In fact, deregulated heme metabolism has been implicated in the pathogenesis of severe sepsis.^{39,48} The proximal tubules are especially vulnerable to the damaging effects of free heme because of their robust fluid-phase uptake.⁴⁹

We also showed that macrophage CD14 and TRIF are essential for the induction of renal tubular protection. In the absence of macrophage CD14, endotoxin can still signal through TLR4 to activate the MyD88 pathway. However, CD14 is required for endotoxin to coactivate TRIF signaling.⁵⁰ Therefore, the failure of CD14KO/WT chimeras to mount tubular preconditioning results, in part, from the lack of TRIF activation. This was confirmed by rescuing protection in the CD14KO/WT chimeras with poly (I:C), a ligand of TLR3, and its downstream TRIF pathway.

CD14 is a multifaceted molecule that exists in both membrane-bound and soluble forms. In particular, the loss of membrane-bound CD14 is associated with worse mortality in patients with sepsis.^{51,52} CD14 is important for endotoxin uptake and essential for the phagocytic activity of macrophages.^{25,53} More recently, CD14 was shown to be abundant in normal human urinary exosomes with antimicrobial properties.⁵⁴ Finally, CD14 and the TRIF pathway are implicated in upstream signaling leading to HO1 expression.³⁴ Collectively, these data impart CD14 with unique properties, and it is tempting to speculate about its possible role as an essential intermediary in the macrophage–tubule crosstalk.

At the tubule level, preconditioning manifested as complete abrogation of peroxisomal damage and oxidative stress. We had previously shown that endotoxin injury to the nonpreconditioned kidney targets tubular peroxisomes very early and mitochondria only at later time points.⁹ Renal tubular peroxisomes are understudied organelles that carry the bulk of oxidative metabolic pathways in the tubules, and they are particularly abundant in S2 and S3 segments.^{9,22–24} They are also the segments that exhibit oxidative stress after endotoxin injury. Therefore, it is not surprising that preconditioning resulted in complete preservation of peroxisomes, thus minimizing the potential for these organelles to unleash pathologic reactive species.

In summary, there is strong mounting evidence that endotoxin preconditioning can result in tissue protection concurrent with a preserved ability to contain and fight infections.^{15–17} In that sense, it is fundamentally different from the immunosuppression that characterizes the late stages of sepsis. Therefore, preconditioning is an attractive model to investigate the mechanisms involved in tissue protection. These mechanisms can then be selectively targeted to prevent and treat infection. In this work, we have presented novel evidence that macrophages are essential in mediating the protective effects of preconditioning to the kidney. Characterizing further this macrophage subset and understanding the mechanisms of its crosstalk with the kidney tubules could result in potential therapies for sepsis and sepsis-induced AKI.

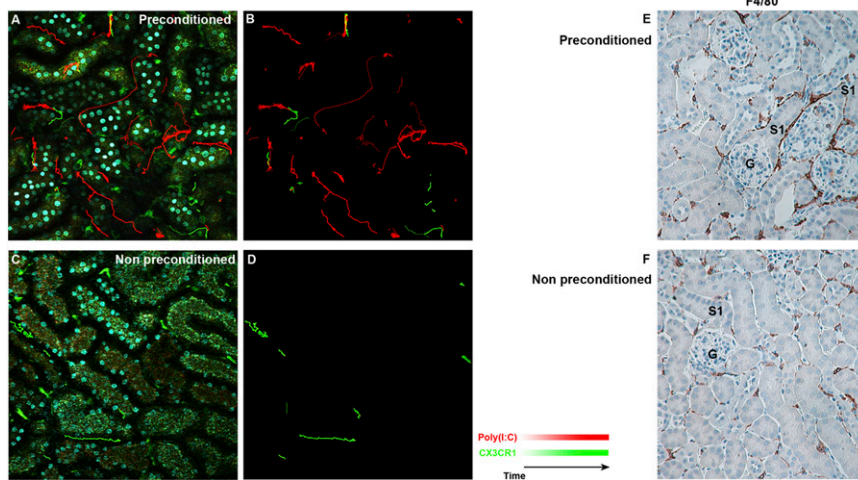


Figure 10. Preconditioning increases the activity and trafficking of macrophages in the kidney. (A) The number and activity of poly (I:C)-positive macrophages were significantly increased in the preconditioned kidney. Mobile macrophages expressing high GFP [poly (I:C)-negative] and intermediate GFP [poly (I:C)-positive] were tracked with computer-generated green and red marks, respectively (Supplemental Movie 1). The isolated tracks are shown in B (Supplemental Movies 2–4 are the original movies without track marks). (C and D) Computer-generated tracking is shown for the non-preconditioned mouse (Supplemental Movies 5 and 6). The tracking of cells with poor cell body delineation or punctate signature was performed with a custom plugin that we developed for ImageJ (Supplemental Table 3). (E and F) Preconditioned and nonpreconditioned kidney tissues were harvested 72 hours after 5 mg/kg LPS ip and stained for F4/80 (brown). F4/80⁺ macrophages are clustered around the S1 proximal tubules in the preconditioned but not the nonpreconditioned kidney. CX₃CR1, CX3C chemokine receptor; G, glomerulus. GFP, green fluorescent protein.

CONCISE METHODS

All animal protocols were approved by Indiana University Institutional Animal Care Committee and conform to the National Institutes of Health Guide for the Care and Use of Laboratory Animals. Male mouse strains C57BL/6J (WT), B6.SJL-Ptpcr^aPepc^b/BoyJ (BoyJ), B6.129S-Cd14^{tm1Frm}/J (CD14^{-/-}), C57BL/6J-Ticam1^{Lps2}/J (TRIF^{-/-}), B6.B10ScN-Tlr4^{lps-del}/JthJ (TLR4^{-/-}), and B6.129P-Cx3cr1^{tm1Litt}/J (CX₃CR1-EGFP) were obtained from The Jackson Laboratory. Mice were 8–12 weeks of age and weighed 20–30 g. Nonpreconditioned animals were subjected to a single dose of 5 mg/kg LPS intraperitoneally (ip). Preconditioned animals were subjected to 0.25 mg/kg LPS ip followed 24 hours later by 5 mg/kg LPS ip (1-day protocol) or 1.25 mg/kg LPS ip followed 72 hours later by 5 mg/kg LPS ip (3-day protocol). Untreated mice received an equivalent dose of sterile normal saline vehicle. LPS from *Salmonella enterica* serotype Minnesota Re 595 (rough strain, L9764; Sigma-Aldrich) and *E. coli* serotype 0111:B4 (smooth strain, L2630; Sigma-Aldrich) was used. Alexa Fluor 568 hydrazide (Life Technologies) was used to label LPS from *S. minnesota* (Re 595; Sigma-Aldrich) using established protocols.⁵⁵ The conjugate was separated from free probe using PD-10 columns (GE Healthcare). Biologic activity of the conjugate was determined through its ability to stimulate TNF- α in cultured macrophages. All findings with our *Salmonella* endotoxin were replicated using Alexa Fluor 594-labeled

endotoxin from *E. coli* (O55:B5; Life Technologies). CX₃CR1-EGFP mice mounted renoprotective preconditioning comparable with C57BL/6J and BoyJ animals. BUN levels were measured using a Trilogy Chemistry Analyzer (Drew Scientific).

Cecal Ligation and Puncture

Under isoflurane anesthesia, the cecum of the mouse was ligated and punctured two times with a 27-gauge needle as we have previously described.³

Macrophage Depletion

Two hundred microliters liposomal clodronate suspension (Encapsula Nano Science) was administered iv 2 hours after 0.25 mg/kg LPS ip. An additional 200 μ l liposomal clodronate was administered iv 2 hours before 5 mg/kg LPS ip.

Live *E. coli* Injection

E. coli was transformed with CFP plasmid (BL21 Star DE3 and pRSET/CFP; Life Technologies). Each animal was injected with approximately 1 million live *E. coli* and euthanized 24 hours later for biochemical analysis.

Intravital Two-Photon Imaging of the Kidney

Live animal imaging was performed using an Olympus FV1000-MPE confocal/multiphoton microscope equipped with a Spectra Physics

MaiTai Deep See laser and gallium arsenide 12-bit detectors. The system is mounted on an Olympus Ix81 inverted microscope stand with a Nikon 20 \times and 60 \times NA 1.2 water-immersion objective. The laser was tuned to 800-nm excitation and used for all studies except for intravital imaging of the CX₃CR1-EGFP mouse with rhodamine-labeled poly (I:C), where 850-nm excitation was used. Animals were placed on the stage with the exposed intact kidney placed in a coverslip-bottomed cell culture dish (HBSt-5040; Warner Instruments) bathed in isotonic saline, which we have previously described.⁵⁶ Oxidative stress was measured in the live mouse with carboxy-H₂DCFDA (carboxy-H₂DCFDA; Life Technologies). Carboxy-H₂DCFDA was administered iv. as a 7-mg/kg bolus from a stock dissolved in ethanol and rediluted in normal saline. Images were collected before injection and 20 minutes after carboxy-H₂DCFDA iv. The degree of oxidative stress was quantitated as we have previously described.⁹ In some experiments, Hoechst (Life Technologies), dissolved in normal saline, was administered ip as a 2-mg/kg bolus 2 hours before imaging. High molecular weight poly (I:C) (Invivogen) was dissolved in endotoxin-free water (1 mg/ml), heated at 68 $^{\circ}$ C for 10 minutes, and then allowed to cool for 1 hour at room temperature; 0.25 mg/kg poly (I:C) was administered ip 24 hours before imaging. In some experiments, rhodamine-conjugated poly (I:C) (Invivogen) was given iv to CX₃CR1-EGFP mice to visualize the distribution of poly (I:C) intravitaly.

Cell Tracking Analysis and Development of a Custom Plugin for ImageJ

The source code is available as a Maven project at <https://github.com/icbm-iupui/track-processing.git> (Supplemental Table 3).

Real-Time Quantitative PCR

RNA extraction from snap-frozen kidneys was performed using Trizol, and approximately 8 μ g RNA was reverse-transcribed using the High Capacity cDNA Reverse Transcription Kit (Life Technologies). TaqMan gene expression assays used include KIM-1 (Mm00506686_m1), NGAL (Mm01324470_m1), and Nox4 (Mm00479246_m1). Real-time quantitative PCR amplifications were performed for 40 cycles using the 7500 Real-Time PCR Systems (Life Technologies). The $\Delta\Delta$ Ct method was used to analyze the relative changes in gene expression. Glyceraldehyde-3-phosphate dehydrogenase was used as an endogenous control for normalization.

Generation of Chimeric Mice

The procedure was performed at the Wells Cancer Center at Indiana University. Recipient mice were irradiated through a 139-Cs source with 1100 cGy total given in two divided doses. Approximately 1 million bone marrow cells obtained from the long bones of donor mice were transplanted through the lateral tail vein. Eight weeks after bone marrow transfer, the degree of chimerism was assessed by flow cytometry using fluorescently labeled TLR4 or CD14 antibodies. Alternatively, chimeric mice were generated between TLR4^{-/-} or CD14^{-/-} mice and BoyJ background strains. BoyJ mice are identical to C57BL/6J, except for the CD45.1 antigen, which is easier to detect by flow cytometry (TLR4 clone MTS510; eBioscience and CD45.1 clone A20 and CD45.2 clone 104; Becton Dickinson). Only animals with chimerism exceeding 96% were used. WT to WT and KO to KO chimeras behaved essentially as WT and KO mice.

Isolation of Cells from Kidneys and Flow Cytometry

Kidneys were harvested, homogenized, and incubated with collagenase type IA (Sigma-Aldrich) in HBSS with Ca and Mg. The digested tissue suspension was passed through a 70- μ m strainer (BD Falcon). A density separation medium, Lympholyte-M (Cedarlane), was used to eliminate erythrocytes as per the manufacturer's instructions. After blocking nonspecific Fc binding with anti-mouse CD16/32 (Clone 93; eBioscience), suspensions were incubated with CD45 (30-F11; BD Pharmingen) followed by goat anti-rat IgG MicroBeads (Miltenyi Biotec). CD45⁺ cell fraction was enriched using MACS (Miltenyi Biotec) according to the manufacturer's protocol. After the enrichment procedure, the following primary antibodies (from eBioscience unless specified otherwise) were added in various combinations: anti-mouse F4/80 (BM8), CD11b (M1/70), CD206 (MR5D3; AbD Serotec), CD11c (N418), F4/80 (BM8), CD4 (RM4-5), CD8 (53-6.7; BD Pharmingen), NK1.1 (PK136), CD19 (1D3), CD3 (17A2), B220 (RA3-6B2), and MHC class II (I-1/I-E, M5/114.15.2). These antibodies were conjugated with eFluor 450, FITC, PE, PE-Cy7, Alexa 647, and APC-Cy7 in various combinations, and their concentrations were titrated before use. To ensure the threshold for CD206 positivity, kidney and peritoneal cells were stained with all reagents except for CD206 antibody (fluorescence - 1 control). A gating strategy to

analyze M1 and M2 phenotypes is shown in Supplemental Figure 6. Propidium iodide was used to exclude dead cells. Detection of the cell surface antigens by flow cytometry was performed on an LSR II (Becton Dickinson) with analysis using Flow Jo software (Treestar).

Proteomic Analyses

Two-dimensional difference gel electrophoresis was performed at Applied Biomix in Hayward, CA. In brief, equal amounts of protein extracts from each kidney tissue and sera (sham, nonpreconditioned, and preconditioned) were labeled with Cy2, -3, or -5, mixed, and separated on a two-dimensional gel. In-gel and crossgel data analyses were performed using DeCyder software. A fold change >2.0 was used as a cutoff in the DeCyder analysis, with which a total of 63 (kidney) and 103 (sera) spots were identified. Protein spots of interest were digested and extracted from the gel and identified by mass spectrometry (MS; MALDI-TOF). Protein identification was on the basis of peptide fingerprint mass mapping (using MS data) and peptide fragmentation mapping (using MS/MS data). The MASCOT search engine was used to identify proteins from primary sequence databases. Prdx5 (Figure 3), haptoglobin, transferrin, and hemopexin (Figure 9) were identified with Protein Score 100% confidence and Total Ion 100% confidence (Supplemental Tables 1 and 2).

Western Blotting

Western blotting of kidney macrophages was conducted after enrichment of a CD11b⁺F4/80⁺ macrophage fraction using MACS (Miltenyi Biotec; three animals were pooled for each condition). The remaining negatively selected kidney tissue (CD11b⁻F4/80⁻) from the same animal was analyzed simultaneously. Proteins were extracted with 1% SDS. Total protein levels were determined using the BCA assay (Pierce). Equal amounts of proteins (20 or 40 μ g) were separated by electrophoreses on 4%–12% Tris-Glycine gels (Life Technologies) and transferred to PVDF membranes. PVDF membranes were blocked with 10% newborn calf serum, incubated with primary antibodies overnight and secondary antibodies for 1 hour, and visualized by chemiluminescence (Thermo Fisher Scientific). The following primary antibodies were used for Western blotting: SIRT1 (ab12193; Abcam), HO1 (ab13243; Abcam, Inc.), Histone H3 (4499; Cell Signaling Technology), and Actin (ab3280; Abcam, Inc.).

Immunohistochemical and Immunofluorescence

Microscopy

Kidneys were fixed with 4% paraformaldehyde and subsequently processed for standard histochemistry or immunofluorescence staining (100- μ m vibratome sections permeabilized with 0.1% Triton X-100). The following primary antibodies were used: HO1 (ab13243; Abcam, Inc.), SIRT1 (ab12193; Abcam, Inc.), catalase (ab1877; Abcam, Inc.), Prdx5 (ABC281; EMD Millipore), F4/80 (Clone Cl:A3-1; AbD Serotec), and Gr-1 (NIMP-R14; Abcam, Inc.). Sections were counterstained with labeled secondary antibodies, FITC phalloidin and DAPI and imaged with an Olympus FV1000-MPE confocal/multiphoton microscope or Nikon Microphot-SA equipped with an SPOT RT Slider camera (Diagnostic Instruments, Inc.). Terminal deoxynucleotidyl transferase-mediated digoxigenin-deoxyuridine nick-end labeling staining was performed

using an ApopTag Red *In Situ* Apoptosis Detection Kit (EMD Millipore) on paraffin-embedded tissues with antigen retrieval as described previously.⁵⁷

Quantification of Cytokines and Chemokines

Analysis of serum and kidney homogenate cytokines/chemokines was performed at EMD Millipore using Milliplex MAP Mouse Cytokine/Chemokine Magnetic Bead Panel– Premixed 32 Plex. Two analytes (IL-6 and IL-13 from kidney homogenates and G-CSF and IL-6 from serum) were omitted from the final analysis in Figure 1 because of out-of-range values. Volcano graphs and heat maps were generated with R software 2.15.2 (heatmap.2{gplots}).

Statistical Analyses

Data were analyzed for statistical significance with R software 2.15.2 using ANOVA and pairwise *t* tests with Holm *P* value adjustment. Significance was set at *P*<0.05. All data are reported as means with SD.

ACKNOWLEDGMENTS

This work was supported by National Institutes of Health Grant R01-DK080067 (to P.C.D.), National Institutes of Health O'Brien Center Grant P30-DK079312 (to P.C.D.), and Dialysis Clinics Inc. (P.C.D.).

DISCLOSURES

None.

REFERENCES

- Murugan R, Kellum JA: Acute kidney injury: What's the prognosis? *Nat Rev Nephrol* 7: 209–217, 2011
- Dellinger RP, Levy MM, Carlet JM, Bion J, Parker MM, Jaeschke R, Reinhart K, Angus DC, Brun-Buisson C, Beale R, Calandra T, Dhainaut JF, Gerlach H, Harvey M, Marini JJ, Marshall J, Ranieri M, Ramsay G, Sevransky J, Thompson BT, Townsend S, Vender JS, Zimmerman JL, Vincent JL; International Surviving Sepsis Campaign Guidelines Committee; American Association of Critical-Care Nurses; American College of Chest Physicians; American College of Emergency Physicians; Canadian Critical Care Society; European Society of Clinical Microbiology and Infectious Diseases; European Society of Intensive Care Medicine; European Respiratory Society; International Sepsis Forum; Japanese Association for Acute Medicine; Japanese Society of Intensive Care Medicine; Society of Critical Care Medicine; Society of Hospital Medicine; Surgical Infection Society; World Federation of Societies of Intensive and Critical Care Medicine: Surviving Sepsis Campaign: International guidelines for management of severe sepsis and septic shock: 2008. *Crit Care Med* 36: 296–327, 2008
- El-Achkar TM, Huang X, Plotkin Z, Sandoval RM, Rhodes GJ, Dagher PC: Sepsis induces changes in the expression and distribution of Toll-like receptor 4 in the rat kidney. *Am J Physiol Renal Physiol* 290: F1034–F1043, 2006
- Wu H, Chen G, Wyburn KR, Yin J, Bertolino P, Eris JM, Alexander SI, Sharland AF, Chadban SJ: TLR4 activation mediates kidney ischemia/reperfusion injury. *J Clin Invest* 117: 2847–2859, 2007
- Pulskens WP, Teske GJ, Butter LM, Roelofs JJ, van der Poll T, Florquin S, Leemans JC: Toll-like receptor-4 coordinates the innate immune response of the kidney to renal ischemia/reperfusion injury. *PLoS ONE* 3: e3596, 2008
- Tsuboi N, Yoshikai Y, Matsuo S, Kikuchi T, Iwami K, Nagai Y, Takeuchi O, Akira S, Matsuguchi T: Roles of toll-like receptors in C-C chemokine production by renal tubular epithelial cells. *J Immunol* 169: 2026–2033, 2002
- Good DW, George T, Watts BA 3rd: Lipopolysaccharide directly alters renal tubule transport through distinct TLR4-dependent pathways in basolateral and apical membranes. *Am J Physiol Renal Physiol* 297: F866–F874, 2009
- Wolfs TG, Buurman WA, van Schadewijk A, de Vries B, Daemen MA, Hiemstra PS, van 't Veer C: In vivo expression of Toll-like receptor 2 and 4 by renal epithelial cells: IFN-gamma and TNF-alpha mediated up-regulation during inflammation. *J Immunol* 168: 1286–1293, 2002
- Kalakeche R, Hato T, Rhodes G, Dunn KW, El-Achkar TM, Plotkin Z, Sandoval RM, Dagher PC: Endotoxin uptake by S1 proximal tubular segment causes oxidative stress in the downstream S2 segment. *J Am Soc Nephrol* 22: 1505–1516, 2011
- Chao W: Toll-like receptor signaling: A critical modulator of cell survival and ischemic injury in the heart. *Am J Physiol Heart Circ Physiol* 296: H1–H12, 2009
- Lehner MD, Ittner J, Bundschuh DS, van Rooijen N, Wendel A, Hartung T: Improved innate immunity of endotoxin-tolerant mice increases resistance to Salmonella enterica serovar typhimurium infection despite attenuated cytokine response. *Infect Immun* 69: 463–471, 2001
- Foster SL, Hargreaves DC, Medzhitov R: Gene-specific control of inflammation by TLR-induced chromatin modifications. *Nature* 447: 972–978, 2007
- Slofstra SH, ten Cate H, Spek CA: Low dose endotoxin priming is accountable for coagulation abnormalities and organ damage observed in the Schwartzman reaction. A comparison between a single-dose endotoxemia model and a double-hit endotoxin-induced Schwartzman reaction. *Thromb J* 4: 13, 2006
- Biswas SK, Lopez-Collazo E: Endotoxin tolerance: New mechanisms, molecules and clinical significance. *Trends Immunol* 30: 475–487, 2009
- Wheeler DS, Lahni PM, Denenberg AG, Poynter SE, Wong HR, Cook JA, Zingarelli B: Induction of endotoxin tolerance enhances bacterial clearance and survival in murine polymicrobial sepsis. *Shock* 30: 267–273, 2008
- Shi DW, Zhang J, Jiang HN, Tong CY, Gu GR, Ji Y, Summah H, Qu JM: LPS pretreatment ameliorates multiple organ injuries and improves survival in a murine model of polymicrobial sepsis. *Inflamm Res* 60: 841–849, 2011
- Lehner MD, Hartung T: Endotoxin tolerance-mechanisms and beneficial effects in bacterial infection. *Rev Physiol Biochem Pharmacol* 144: 95–141, 2002
- Godet C, Goujon JM, Petit I, Lecron JC, Hauet T, Mauco G, Carretier M, Robert R: Endotoxin tolerance enhances interleukin-10 renal expression and decreases ischemia-reperfusion renal injury in rats. *Shock* 25: 384–388, 2006
- Heemann U, Szabo A, Hamar P, Müller V, Witzke O, Lutz J, Philipp T: Lipopolysaccharide pretreatment protects from renal ischemia/reperfusion injury: Possible connection to an interleukin-6-dependent pathway. *Am J Pathol* 156: 287–293, 2000
- Vogt BA, Alam J, Croatt AJ, Vercellotti GM, Nath KA: Acquired resistance to acute oxidative stress. Possible role of heme oxygenase and ferritin. *Lab Invest* 72: 474–483, 1995
- Zager RA, Johnson AC, Lund S: 'Endotoxin tolerance': TNF-alpha hyper-reactivity and tubular cytoresistance in a renal cholesterol loading state. *Kidney Int* 71: 496–503, 2007
- Usuda N, Yokota S, Hashimoto T, Nagata T: Immunocytochemical localization of D-amino acid oxidase in the central clear matrix of rat kidney peroxisomes. *J Histochem Cytochem* 34: 1709–1718, 1986

23. Bonekamp NA, Vökl A, Fahimi HD, Schrader M: Reactive oxygen species and peroxisomes: Struggling for balance. *Biofactors* 35: 346–355, 2009
24. Schrader M, Fahimi HD: Peroxisomes and oxidative stress. *Biochim Biophys Acta* 1763: 1755–1766, 2006
25. Zanoni I, Ostuni R, Marek LR, Barresi S, Barbalat R, Barton GM, Granucci F, Kagan JC: CD14 controls the LPS-induced endocytosis of Toll-like receptor 4. *Cell* 147: 868–880, 2011
26. Jiang Z, Georgel P, Du X, Shamel L, Sovath S, Mudd S, Huber M, Kalis C, Keck S, Galanos C, Freudenberg M, Beutler B: CD14 is required for MyD88-independent LPS signaling. *Nat Immunol* 6: 565–570, 2005
27. Vartanian KB, Stevens SL, Marsh BJ, Williams-Karnesky R, Lessov NS, Stenzel-Poore MP: LPS preconditioning redirects TLR signaling following stroke: TRIF-IRF3 plays a seminal role in mediating tolerance to ischemic injury. *J Neuroinflammation* 8: 140, 2011
28. Biswas SK, Bist P, Dhillon MK, Kajiji T, Del Fresno C, Yamamoto M, Lopez-Collazo E, Akira S, Tergaonkar V: Role for MyD88-independent, TRIF pathway in lipid A/TLR4-induced endotoxin tolerance. *J Immunol* 179: 4083–4092, 2007
29. Jung S, Aliberti J, Graemmel P, Sunshine MJ, Kreutzberg GW, Sher A, Littman DR: Analysis of fractalkine receptor CX(3)CR1 function by targeted deletion and green fluorescent protein reporter gene insertion. *Mol Cell Biol* 20: 4106–4114, 2000
30. De Wilde V, Van Rompaey N, Hill M, Lebrun JF, Lemaître P, Lhomme F, Kubjak C, Vokaer B, Oldenhove G, Charbonnier LM, Cuturi MC, Goldman M, Le Moine A: Endotoxin-induced myeloid-derived suppressor cells inhibit alloimmune responses via heme oxygenase-1. *Am J Transplant* 9: 2034–2047, 2009
31. Gozzelino R, Jeney V, Soares MP: Mechanisms of cell protection by heme oxygenase-1. *Annu Rev Pharmacol Toxicol* 50: 323–354, 2010
32. Liu TF, Yoza BK, El Gazzar M, Vachharajani VT, McCall CE: NAD⁺-dependent SIRT1 deacetylase participates in epigenetic reprogramming during endotoxin tolerance. *J Biol Chem* 286: 9856–9864, 2011
33. Shen Z, Ajmo JM, Rogers CQ, Liang X, Le L, Murr MM, Peng Y, You M: Role of SIRT1 in regulation of LPS- or two ethanol metabolites-induced TNF-alpha production in cultured macrophage cell lines. *Am J Physiol Gastrointest Liver Physiol* 296: G1047–G1053, 2009
34. Tzima S, Victoratos P, Kranidioti K, Alexiou M, Kollias G: Myeloid heme oxygenase-1 regulates innate immunity and autoimmunity by modulating IFN-beta production. *J Exp Med* 206: 1167–1179, 2009
35. Zhang Z, Lowry SF, Guarente L, Haimovich B: Roles of SIRT1 in the acute and restorative phases following induction of inflammation. *J Biol Chem* 285: 41391–41401, 2010
36. Ferenbach DA, Nkejabega NC, McKay J, Choudhary AK, Vernon MA, Beesley MF, Clay S, Conway BC, Marson LP, Kluth DC, Hughes J: The induction of macrophage hemeoxygenase-1 is protective during acute kidney injury in aging mice. *Kidney Int* 79: 966–976, 2011
37. Zarjou A, Agarwal A: Sepsis and acute kidney injury. *J Am Soc Nephrol* 22: 999–1006, 2011
38. Tracz MJ, Juncos JP, Grande JP, Croatt AJ, Ackerman AW, Rajagopalan G, Knutson KL, Badley AD, Griffin MD, Alam J, Nath KA: Renal hemodynamic, inflammatory, and apoptotic responses to lipopolysaccharide in HO-1^{-/-} mice. *Am J Pathol* 170: 1820–1830, 2007
39. Larsen R, Gozzelino R, Jeney V, Tokaji L, Bozza FA, Japiassú AM, Bonaparte D, Cavalcante MM, Chora A, Ferreira A, Marguti I, Cardoso S, Sepúlveda N, Smith A, Soares MP: A central role for free heme in the pathogenesis of severe sepsis. *Sci Transl Med* 2: 51ra71, 2010
40. Nathan C, Cunningham-Bussell A: Beyond oxidative stress: An immunologist's guide to reactive oxygen species. *Nat Rev Immunol* 13: 349–361, 2013
41. Wu L, Gokden N, Mayeux PR: Evidence for the role of reactive nitrogen species in polymicrobial sepsis-induced renal peritubular capillary dysfunction and tubular injury. *J Am Soc Nephrol* 18: 1807–1815, 2007
42. Otto GP, Sosso M, Claus RA, Rödel J, Menge K, Reinhart K, Bauer M, Riedemann NC: The late phase of sepsis is characterized by an increased microbiological burden and death rate. *Crit Care* 15: R183, 2011
43. Hutchins NA, Unsinger J, Hotchkiss RS, Ayala A: The new normal: Immunomodulatory agents against sepsis immune suppression. *Trends Mol Med* 20: 224–233, 2014
44. Stearns-Kurosawa DJ, Osuchowski MF, Valentine C, Kurosawa S, Remick DG: The pathogenesis of sepsis. *Annu Rev Pathol* 6: 19–48, 2011
45. Deutschman CS, Tracey KJ: Sepsis: Current dogma and new perspectives. *Immunity* 40: 463–475, 2014
46. Meisel C, Scheffold JC, Pschowski R, Baumann T, Hetzger K, Gregor J, Weber-Carstens S, Hasper D, Keh D, Zuckermann H, Reinke P, Volk HD: Granulocyte-macrophage colony-stimulating factor to reverse sepsis-associated immunosuppression: A double-blind, randomized, placebo-controlled multicenter trial. *Am J Respir Crit Care Med* 180: 640–648, 2009
47. Monneret G, Venet F, Pachot A, Lepape A: Monitoring immune dysfunctions in the septic patient: A new skin for the old ceremony. *Mol Med* 14: 64–78, 2008
48. Schaefer DJ, Buehler PW, Alayash AI, Belcher JD, Vercellotti GM: Hemolysis and free hemoglobin revisited: Exploring hemoglobin and heme scavengers as a novel class of therapeutic proteins. *Blood* 121: 1276–1284, 2013
49. Baek JH, D'Agnillo F, Vellelian F, Pereira CP, Williams MC, Jia Y, Schaefer DJ, Buehler PW: Hemoglobin-driven pathophysiology is an in vivo consequence of the red blood cell storage lesion that can be attenuated in guinea pigs by haptoglobin therapy. *J Clin Invest* 122: 1444–1458, 2012
50. Beutler B, Jiang Z, Georgel P, Crozat K, Croker B, Rutschmann S, Du X, Hoebe K: Genetic analysis of host resistance: Toll-like receptor signaling and immunity at large. *Annu Rev Immunol* 24: 353–389, 2006
51. Aalto H, Takala A, Kautiainen H, Siitonen S, Repo H: Monocyte CD14 and soluble CD14 in predicting mortality of patients with severe community acquired infection. *Scand J Infect Dis* 39: 596–603, 2007
52. Venet F, Pachot A, Debard AL, Bohe J, Bienvenu J, Lepape A, Powell WS, Monneret G: Human CD4⁺CD25⁺ regulatory T lymphocytes inhibit lipopolysaccharide-induced monocyte survival through a Fas/Fas ligand-dependent mechanism. *J Immunol* 177: 6540–6547, 2006
53. Zanoni I, Granucci F: Role of CD14 in host protection against infections and in metabolism regulation. *Front Cell Infect Microbiol* 3: 32, 2013
54. Hiemstra TF, Charles PD, Gracia T, Hester SS, Gatto L, Al-Lamki R, Floto RA, Su Y, Skepper JN, Lilley KS, Karet Frankl FE: Human urinary exosomes as innate immune effectors [published online ahead of print April 3, 2014]. *J Am Soc Nephrol*
55. Triantafilou K, Triantafilou M, Fernandez N: Lipopolysaccharide (LPS) labeled with Alexa 488 hydrazide as a novel probe for LPS binding studies. *Cytometry* 41: 316–320, 2000
56. Dunn KW, Sandoval RM, Kelly KJ, Dagher PC, Tanner GA, Atkinson SJ, Bacallao RL, Molitoris BA: Functional studies of the kidney of living animals using multicolor two-photon microscopy. *Am J Physiol Cell Physiol* 283: C905–C916, 2002
57. Sutton TA, Hato T, Mai E, Yoshimoto M, Kuehl S, Anderson M, Mang H, Plotkin Z, Chan RJ, Dagher PC: p53 is renoprotective after ischemic kidney injury by reducing inflammation. *J Am Soc Nephrol* 24: 113–124, 2013

See related editorial, "Endotoxin and AKI: Macrophages Protect after Preconditioning," on pages 1231–1232.

This article contains supplemental material online at <http://jasn.asnjournals.org/lookup/suppl/doi:10.1681/ASN.2014060561/-/DCSupplemental>.